SUPPLEMENTARY INFORMATION

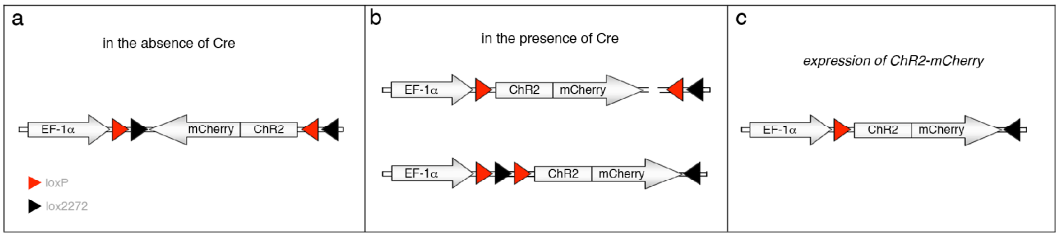

Supplementary Figure 1. Cre dependent expression of the light-activated channel ChR2 (a) The adeno-associated viral vector AAV DIO ChR2-mCherry carries an inverted version of ChR2 fused to the fluorescent marker mCherry. This strategy prevents ChR2 from being expressed in the absence of Cre. (b) The loxP variants loxP and lox2272 flanking ChR2-mCherry are incompatible and cannot recombine with each other[1], leading to a stochastic recombination of either variant[2] in the presence of Cre. Because both loxP variants are constituted of lox pairs facing each other, recombination results in inversion of ChR2-mCherry into the sense orientation. As a consequence of the first recombination event, the second unrecombined loxP variant now is constituted of two directly oriented lox sites and will therefore excise one of the lox sites of the first loxP variant, an event that prevents further recombination. (c) This strategy eliminates possible misexpression of ChR2 due to leakiness of the commonly used translational stop cassettes and targets recombination and expression of ChR2-mCherry exclusively to Cre expressing cells.

1. Lee, G. & Saito, I. Role of nucleotide sequences of loxP spacer region in Cre-mediated recombination. *Gene* **216**, 55-65 (1998).
2. Livet, J. et al. Transgenic strategies for combinatorial expression of fluorescent proteins in the nervous system. *Nature* **450**, 56-62 (2007).

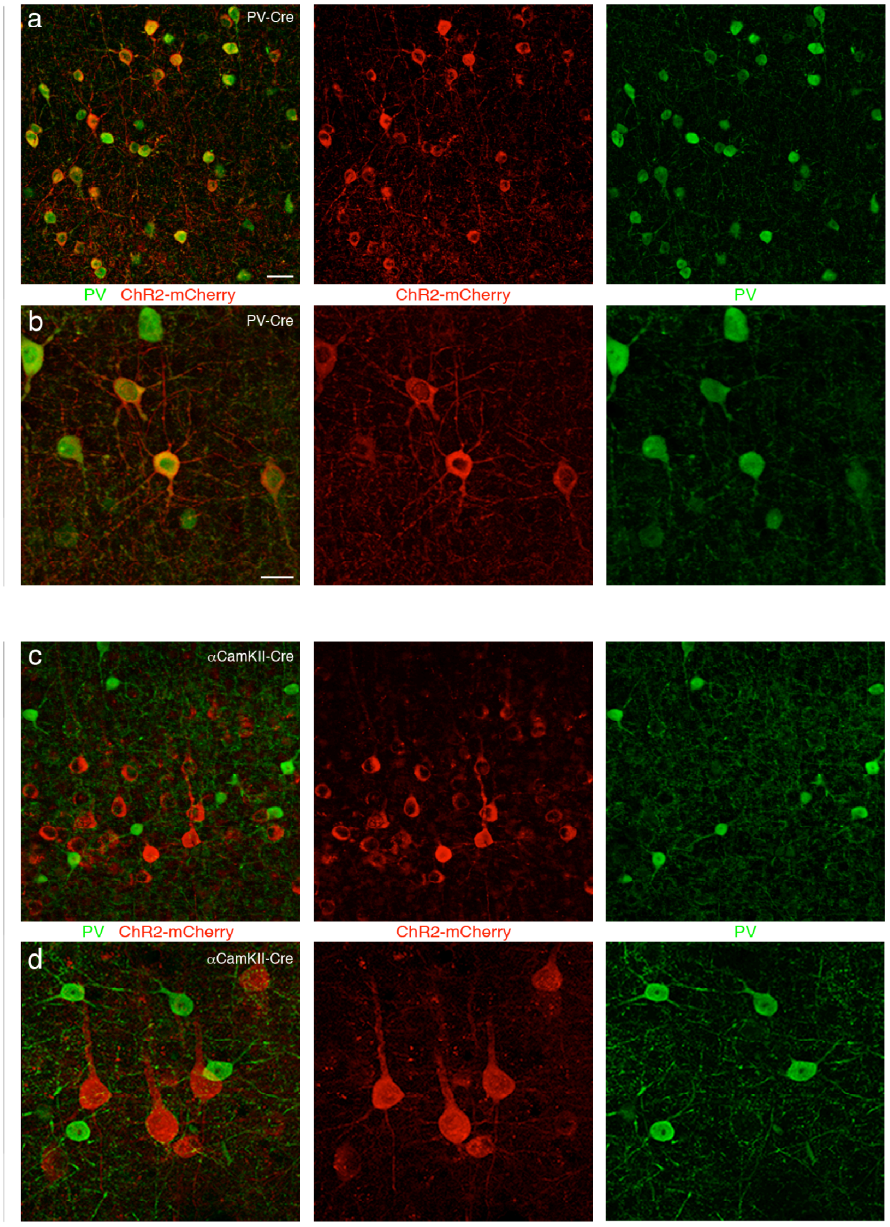

Supplementary Figure 2. Cell type-specific expression of ChR2 in the adult barrel cortex. (a) When injected into the barrel cortex of adult PV-Cre mice, the viral vector AAV DIO ChR2-mCherry gave robust expression of ChR2 in PV^+ interneurons throughout cortical layers. (b) Confocal Z-stack showing PV^+ cells with ChR2-mCherry expression and typical FS interneuron morphology. (c-d) A corresponding injection into the barrel cortex of αCamKII-Cre mice resulted in exclusive labeling of excitatory neurons. (c) ChR2-mCherry expression in αCamKII-Cre mice was confined to excitatory neurons immune-negative for parvalbumin (PV). (d) Confocal Z-stack showing ChR2-mCherry expressing cells with typical pyramidal neuron morphology. Scale bars are the same in (a, c; 25 μm) and (b, d; 25 μm).

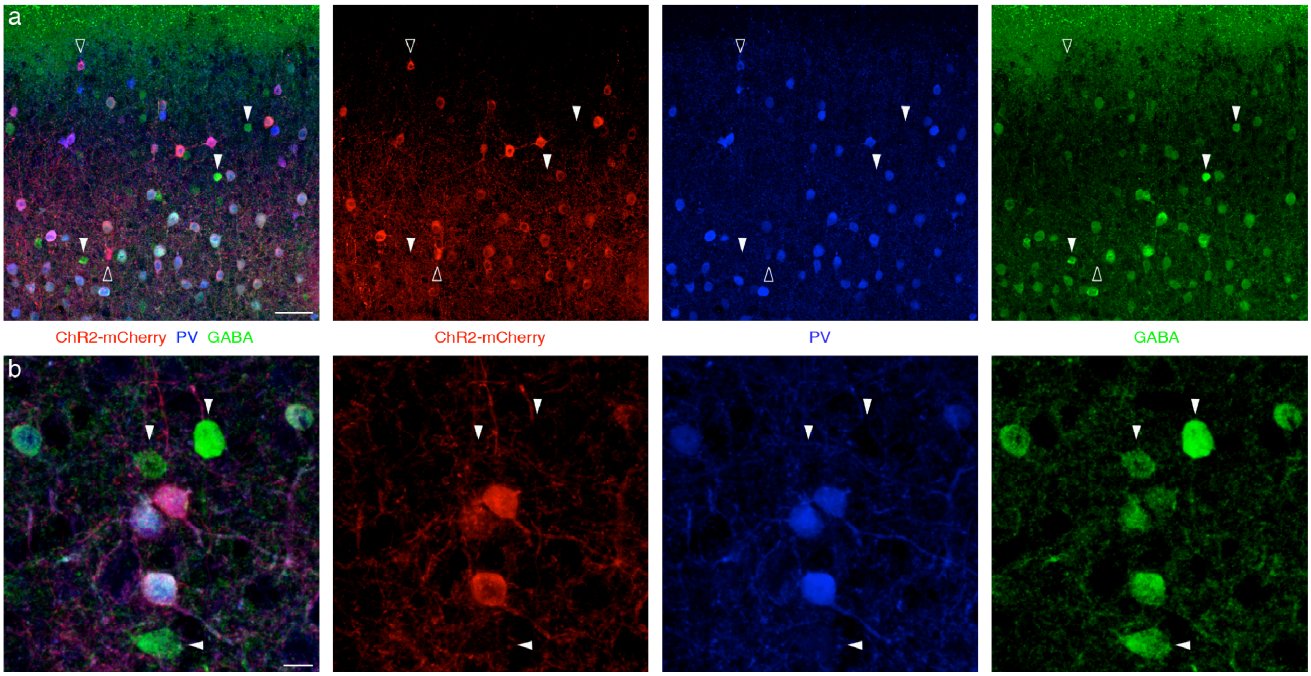

Supplementary Figure 3. ChR2-mCherry expressing cells in PV-Cre mice are PV+ interneurons that express the inhibitory neurotransmitter GABA. (a-b) After injection of AAV DIO ChR2-mCherry into the barrel cortex of adult PV-Cre mice, expression of light-activated channels is found in GABAergic PV+ interneurons. (a) Confocal Z-stack of triple labeled cells in layer 2/3. Virtually all cells expressing ChR2-mCherry show detectable levels of PV and GABA. In the instance of low/non-detectable levels of GABA (hollow arrowheads) the ChR2-mCherry+ cells still show detectable levels of PV. White arrowheads point to GABAergic interneurons (GABA+) not expressing the Ca^{2+}-binding protein PV and therefore also lacking expression of light-activated channels. (b) High-magnification confocal Z-stack of triple labeled cells. GABAergic PV- interneurons are clearly lacking expression of ChR2-mCherry (white arrowheads). Scale bar is 50 μm in (a) and 10 μm in (b).

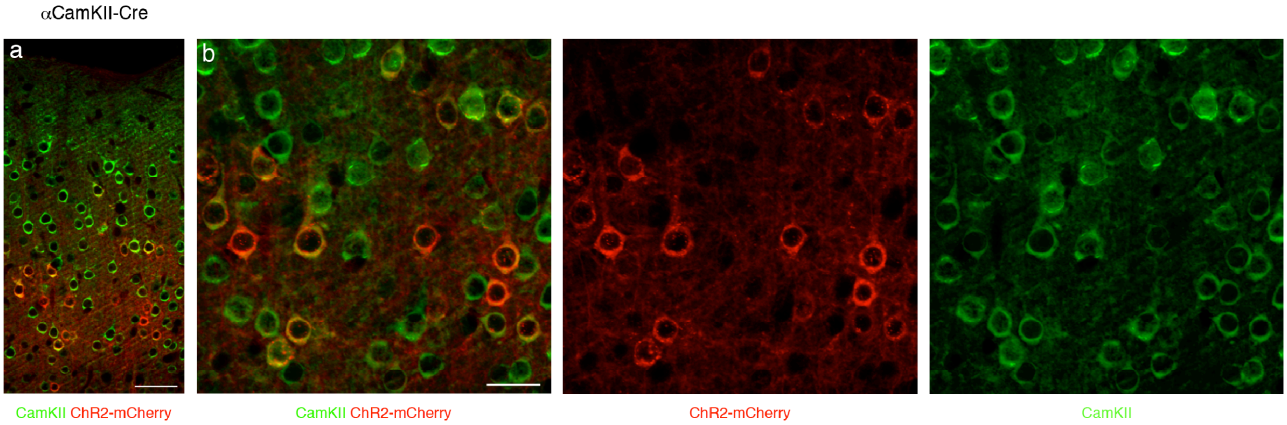

Supplementary Figure 4. ChR2-mCherry expressing cells in αCamKII-Cre mice are CamKII$^+$ excitatory neurons . (a-b) After injection of AAV DIO ChR2-mCherry into the barrel cortex of adult αCamKII-Cre mice, expression of light-activated channels is restricted to CamKII$^+$ excitatory neurons. (a) One 3 μm section of layer 2/3. (b) Part of (a) in high-magnification, showing that ChR2-mCherry expressing neurons are immunopositive for the excitatory marker CamKII. Scale bar is 50 μm in (a) and 25 μm in (b).

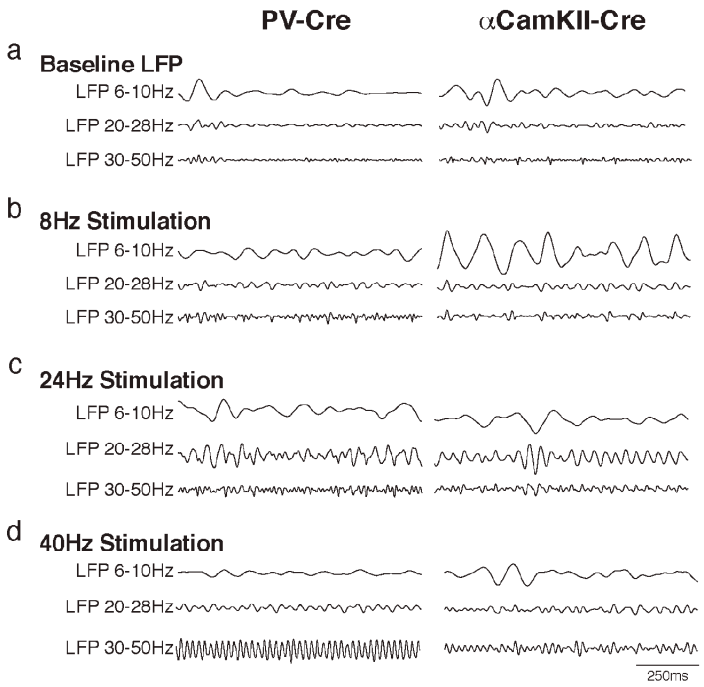

Supplementary Figure 5. Examples of LFP traces from PV-Cre and αCamKII-Cre mice during baseline activity and varying frequencies of light stimulation.
(a) Baseline LFP recordings from barrel cortex in the absence of light stimulation. (b) Stimulation at 8 Hz evoked increased 8 Hz activity in αCamKII-Cre but not PV-Cre mice, but did not affect activity in the 24 or 40 Hz bands in either type of mouse. (c) Similarly, 24 Hz stimulation evoked a small increase in 24 Hz activity in both types of mouse but did not affect other frequency bands. (d) Stimulation at 40 Hz evoked a large 40 Hz oscillation in the PV-Cre mouse, but did not affect activity in any frequency band in the αCamKII-Cre mouse.

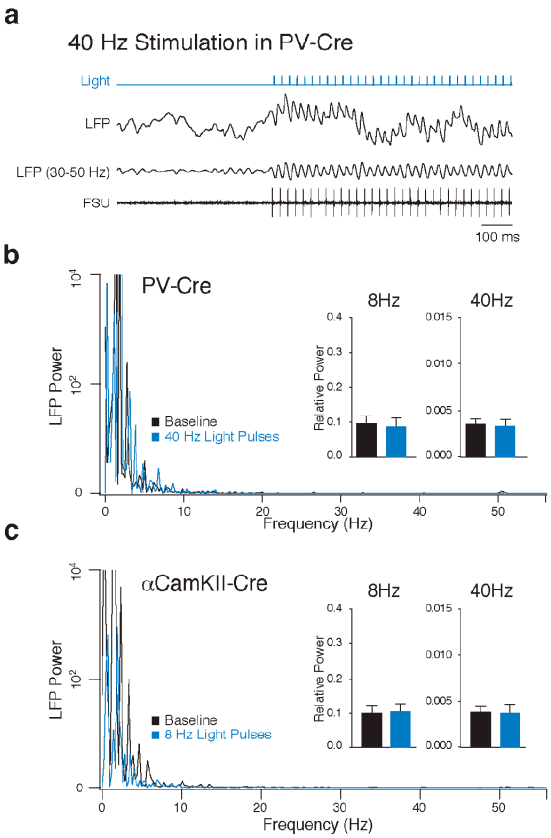

Supplementary Figure 6. Light stimulation evokes LFP activity only in transduced tissue expressing ChR2. (a) LFP and single unit FS interneuron recording in a PV-Cre animal during 40 Hz stimulation with light pulses. Light pulses evoked a robust gamma oscillation in the LFP, which can be seen clearly in the trace filtered between 30 and 50 Hz. The recorded FSU fired one spike in response to each light pulse. (b) Light stimulation at 40 Hz did not affect the LFP in barrel cortex of the untransduced hemisphere of PV-Cre animals. In this example (left), there was no difference in LFP power in any frequency band between baseline (black) and 40 Hz light stimulation (blue) conditions. The bar graphs (right) show population averages (n = 6 animals) for LFP power in the 8 and 40 Hz frequency bands during baseline (black) and light stimulation (blue) of untransduced cortex. (c) Similarly, 8 Hz light stimulation in barrel cortex of the untransduced hemisphere of an αCamKII-Cre animal had no impact on LFP power in this example (left). Across the population, there was no impact of light stimulation in either the 8 or 40 Hz bands (n = 5 animals; right).

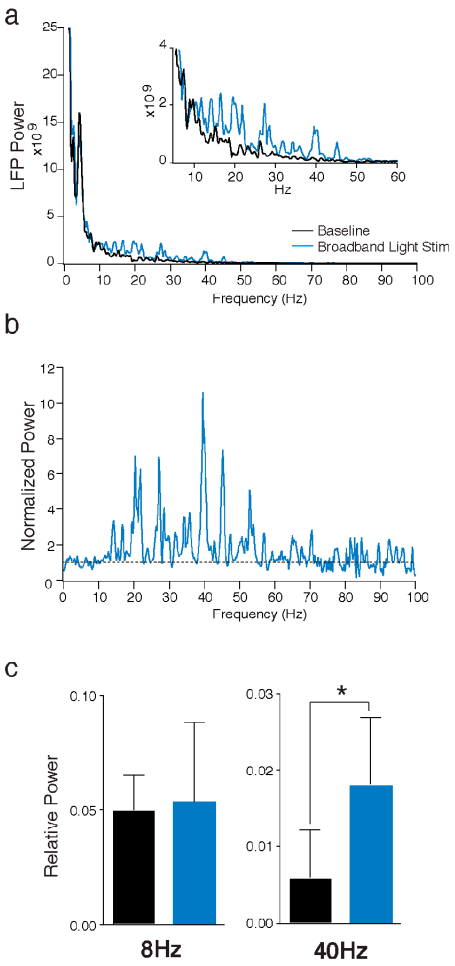

Supplementary Figure 7. Broadband light stimulation evoked LFP activity in the gamma range. (a) The broadband stimulus (5-200 Hz) evoked an increase in LFP power that was specific to the gamma range (20-80 Hz), even though the stimulus contained many other frequencies. Inset traces show an expanded portion of the LFP power spectra. Baseline power spectrum is shown in black, power spectrum during broadband light stimulation is shown in blue. (b) LFP power spectrum during broadband stimulation, normalized to the baseline power spectrum. (c) Relative LFP power in the 8 Hz (left) and 40 Hz (right) frequency bands during baseline activity (black) and broadband light stimulation (blue). Relative power was unaffected in the 8 Hz band, but was significantly increased in the 40 Hz band (n = 7 sites in 4 animals; $p < 0.05$).

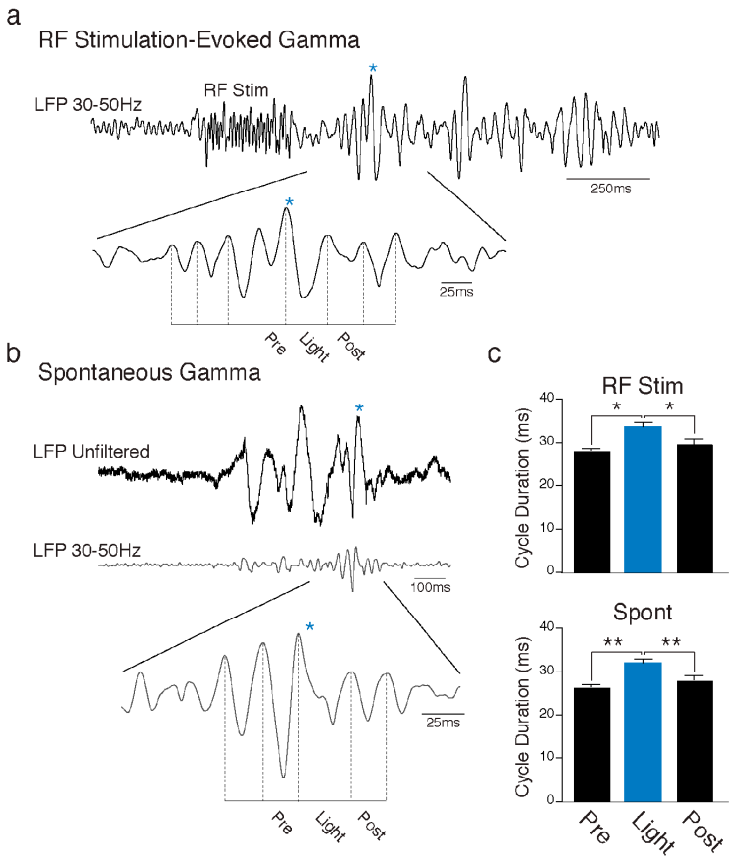

Supplementary Figure 8. Brief stimulation of FS cells during naturally occurring gamma shifts the phase of the ongoing oscillation. (a) Stimulation of the midbrain reticular formation (RF) led to increased gamma activity (n = 18 trials, 2 animals). A brief light pulse was given during an ongoing gamma oscillation (blue asterisk), prolonging the ongoing gamma cycle and shifting the phase of the following cycles relative to the pre-light oscillation. (b) FS stimulation during naturally occurring gamma observed during spontaneous LFP activity (n = 26 trials, 4 animals). Upper trace: unfiltered example of LFP activity. Center trace: gamma frequency band. Lower trace: enlarged portion of the filtered LFP, with a brief pulse of light denoted by the blue asterisk. (c) FS activation by the light pulse significantly increased the duration of the ongoing gamma cycle (Light) in comparison to the preceding (Pre) and following (Post) cycles during gamma oscillations evoked by RF stimulation (Kruskal-Wallis test with Dunn's post-test; $p < 0.05$). Similarly, FS activation increased the duration of the ongoing gamma cycle during spontaneous gamma oscillations, as shown in the example in (b) ($p < 0.01$).

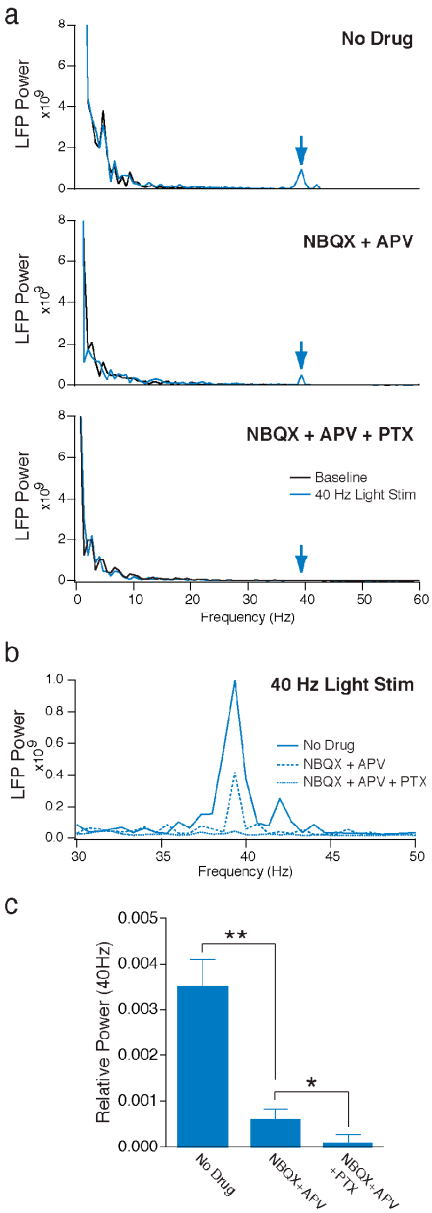

Supplementary Figure 9. Gamma oscillations induced by FS activation require excitatory synaptic activity. (a) Upper panel: LFP power spectra from a PV-Cre animal in the absence of pharmacological manipulation, showing robust gamma activity evoked by 40 Hz light stimulation (arrows). Middle Panel: LFP power spectra after blockade of AMPA and NMDA receptors with NBQX and APV, respectively. Lower Panel: LFP power spectra after additional blockade of GABAa receptors by picrotoxin. (b) Enlarged overlay of the gamma range of the LFP power spectra during light stimulation under each pharmacological condition. (c) Blockade of AMPA and NMDA receptors significantly decreased the relative power evoked in the gamma frequency band by the light (n = 4 sites in 4 animals; $p < 0.01$). The remaining 40 Hz activity in the LFP was eliminated by further blockade of GABAa receptors ($p < 0.05$).

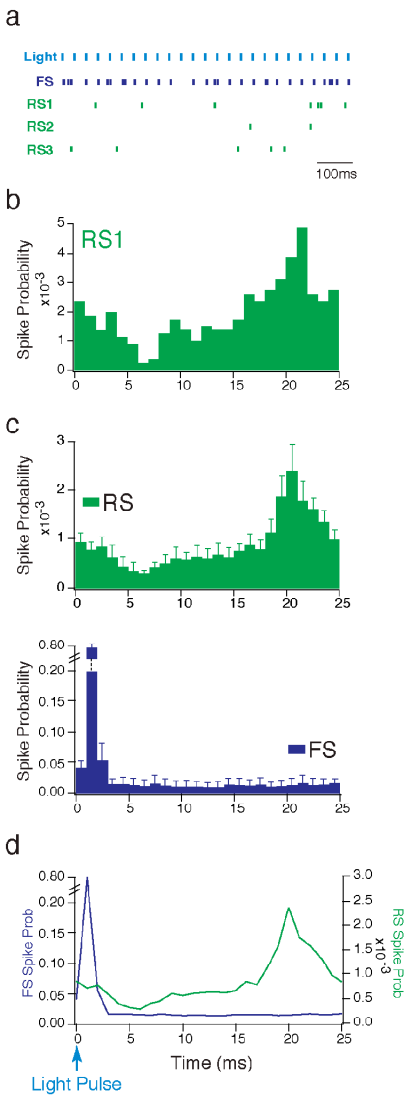

Supplementary Figure 10. Gamma oscillations rhythmically entrain spontaneous RS activity. (a) Raster plot from one experiment, showing repeated activation of an FS cell (blue) by light pulses. Three nearby RS cells were recorded simultaneously (RS1-3, green). (b) Cycle histogram of the spiking activity of RS1 from (a), with 0 set as the time of the light flash on each cycle. (c) Upper panel: Population cycle histogram from 17 RS cells in 5 PV-Cre animals, showing a decrease in spike probability around 4-10 ms after the light flash and an increase in spike probability around 20 ms. Lower panel: Population cycle histogram from 9 FS cells recorded in the same experiments, showing a light-evoked peak in firing at 1-2 ms. (d) Overlay of the FS (blue) and RS (green) spike probability profiles. Light pulses at 0 ms evoked FS spikes with a delay of 1-2 ms, followed by an increase in RS spiking at 17-24 ms.

Supplementary Methods

AAV-DIO-ChR2-mCherry

This vector carries an inverted version of ChR2 fused to the fluorescent marker mCherry to prevent ChR2 from being expressed in the absence of Cre. ChR2-mCherry is flanked by a pair of canonical loxP sites (loxP) and a pair of mutated loxP sites (lox2272). In the presence of Cre, ChR2-mCherry is inverted into the sense direction and expressed from the EF1-α promoter.

In vitro characterization

HEK293 cells (ATCC) were cultured in IMDM (Invitrogen) and 10% FBS (Hyclone) in the presence of gentamycin (Invitrogen). *In vitro* transduction of HEK293 cells with AAV DIO ChR2-mCherry was performed with a serial dilution of viral particles. Cell transfections were performed 7 days later using Lipofectamine 2000 according to manufacturer´s instructions (Invitrogen). For induction of recombination, cells were co-transfected with one plasmid expressing EGFP and one plasmid expressing Cre recombinase in 1:3 ratio. Control cells transduced with virus were transfected with an EGFP expressing plasmid alone. Expression of membrane targeted ChR2-mCherry was scored in an inverted epifluorescent microscope (Nikon) 3 days later.

Extracellular Recordings

Tetrodes and stereotrodes were made from four or two twisted Formvar-coated Tungsten wires (California Fine Wire Company, Grover Beach, CA), respectively, of 12.5 μm diameter each. Online spike discrimination and data acquisition used the Cheetah data acquisition software (Neuralynx, Bozeman MT). Units were hand-separated post-hoc using manual cluster-cutting software (SpikeSort3D, Neuralynx). Cross correlation analysis was used to confirm unit separation. Units that were not easily separable were discarded. Local field potentials were recorded with open filters; units were recorded from data filtered from 600-9000 Hz. All data was sampled at 30kHz.

Spike waveforms of RS and FS cells were characterized, as shown in the examples below, by measuring (1) the ratio between the amplitude of the initial peak (*a*) to the following trough (*b*) and (2) the duration of the spike at half height (*c*). Dotted line indicates mean baseline level in the absence of spikes.

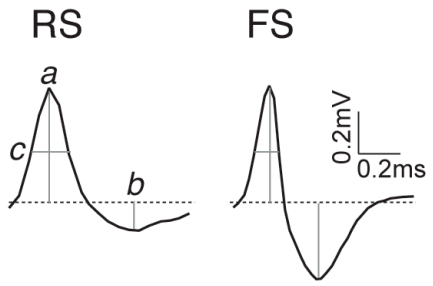

FS and RS spikes were significantly different in both mean spike duration at half height (FS 163.1 ± 3.2 μs, RS 262.4 ± 4.2 μs; unpaired t-test, $p < 0.001$) and peak:trough ratio (FS 1.3 ± 0.03, RS 2.2 ± 0.1; unpaired t-test, $p < 0.001$).

The latency to light-activated FS spikes (median spike latency: Low Power 2.5 ± 0.4 ms, High Power 1.1 ± 0.1 ms; black circles) agreed well with the onset latency of the resulting IPSPs (median onset latency: Low Power 3.2 ± 0.3 ms, High Power 1.6 ± 0.1 ms; open circles). The IPSP time to peak decreased with increasing power (time to peak: Low Power 16.3 ± 1.3 ms, High Power 5.4 ± 0.4 ms; unpaired t-test, $p < 0.05$). Low Power: 46 mW/mm^2, High Power: 68 mW/mm^2.

To minimize possible light-driven artifacts, we employed minimal duration light pulses and took an oblique approach to insertion of the electrodes. The electrodes were typically placed so that the peak light delivery on the surface of the cortex was off-center to the position of electrode entry by ~75-200μm.

Whole-Cell Recordings

Electrodes (5-7MOhm resistance) were pulled on a Sutter P-97 and filled with internal patch solution (130 mM K-Gluconate, 4 mM KCl, 2 mM NaCl, 10 mM Hepes, 0.2 mM EGTA, 10 mM Phosphocreatine, 4 mM MgATP, 0.3 mM Na3GTP, adjusted to pH 7.25 with KOH and 292 mOsm with ddH2O). Electrodes were lowered under

positive pressure while injecting small amplitude current pulses. After formation of a gigaseal, the cell membrane was broken and the whole-cell recording configuration achieved (MultiClamp 700B, Molecular Devices, Sunnyvale CA). After establishing a stable recording, a series of light pulses (1 and 10 ms duration at 3 and 8 mW/mm^2) were presented to evoke FS activity and subsequent IPSPs. In addition, small current pulses were given to measure input resistance, leak conductance (g_L), and leak reversal potential (E_L), and membrane capacitance (C_m). All recordings were stable, with a membrane potential <60mV and steady input resistance. Mean baseline input resistance was 81 ± 16.7 MΩ.

The synaptic reversal potential E_{syn} at the peak of the light-evoked IPSP was calculated as follows. The membrane equation states that the capacitive current in the cell is equal to the sum of all other currents (leak, synaptic and injected):

$$C_m * dV_m/dt = g_L * (E_L - V_m) + g_{syn} * (E_{syn} - V_m) + I_{inj}.$$

In this equation, the synaptic conductance g_{syn} includes both excitatory and inhibitory conductances and the synaptic reversal potential E_{syn} is a weighted sum of the excitatory and inhibitory reversals. This equation can be rewritten to solve for the synaptic current:

$$I_{syn} = g_{syn} * (E_{syn} - V_m) = dV_m/dt * C_m - g_L * (E_L - V_m) - I_{inj}.$$

The right-hand side of this equation can be calculated from experimental data. The membrane potential and its derivative, as well as the injected current, are directly given. Membrane capacitance (C_m), leak conductance (g_L), and leak reversal potential (E_L) were estimated based on response to hyperpolarizing current pulses. According to this equation, the synaptic current I_{syn} is linear in the membrane potential V_m. Because of natural fluctuations in the membrane potential during repeated stimulations, injecting varying levels of current I_{inj} yields a V-I plot. Since I_{syn} is zero if $V_m = E_{syn}$, the synaptic reversal potential can be calculated as the voltage where the best line fit intersects with the x-axis.

Broadband Light Stimulation

For broadband light stimulation we gave 3 sec bouts of 1ms light pulses at frequencies randomly selected from an even distribution 5-200 Hz.

Pharmacology

Baseline LFP and FS spike responses to 40 Hz light stimulation were recorded. The AMPA receptor blocker NBQX and the NMDA receptor APV were then each applied at 50 μM to the surface of the cortex for one hour, after which LFP and spike responses were again characterized. The GABAa receptor blocker picrotoxin was then applied at 50 μM in combination with the NBQX and APV. After an additional hour, LFP and spike responses were again characterized.